Available online at www.sciencedirect.com
SCIENCE DIRECT®
ELSEVIER
International Journal of Solids and Structures 43 (2006) 4810–4829
INTERNATIONAL JOURNAL OF SOLIDS and STRUCTURES
www.elsevier.com/locate/ijsolstr

Nonlinear thermo-elastic buckling characteristics of cross-ply laminated joined conical–cylindrical shells

B.P. Patel [a,*], Y. Nath [a], K.K. Shukla [b]

[a] *Indian Institute of Technology, Department of Applied Mechanics, Hauz Khas, New Delhi 110 016, India*
[b] *Motilal Nehru National Institute of Technology, Allahabad 211 004, India*

Received 7 April 2005
Available online 26 September 2005

Abstract

Here, the nonlinear thermo-elastic buckling/post-buckling characteristics of laminated circular conical–cylindrical/conical–cylindrical–conical joined shells subjected to uniform temperature rise are studied employing semi-analytical finite element approach. The nonlinear governing equations, considering geometric nonlinearity based on von Karman's assumption for moderately large deformation, are solved using Newton–Raphson iteration procedure coupled with displacement control method to trace the pre-buckling/post-buckling equilibrium path. The presence of asymmetric perturbation in the form of small magnitude load spatially proportional to the linear buckling mode shape is assumed to initiate the bifurcation of the shell deformation. The study is carried out to highlight the influences of semi-cone angle, material properties and number of circumferential waves on the nonlinear thermo-elastic response of the different joined shell systems.

Keywords: Joined shells; Conical–cylindrical–conical; Cross-ply; Thermal post-buckling; Critical temperature; Bifurcation; Semi-analytical finite element

1. Introduction

The joined conical–cylindrical shells have wide spread applications in mechanical, marine, aeronautical, chemical, civil and power engineering. They may consist of thin-walled structures composed of two or more simple components having one common axis of revolution and presenting a slope discontinuity in the shell

* Corresponding author. Tel.: +91 011 26591232; fax: +91 011 26581119.
E-mail address: badripatel@hotmail.com (B.P. Patel).

0020-7683/$ - see front matter © 2005 Elsevier Ltd. All rights reserved.
doi:10.1016/j.ijsolstr.2005.07.025

meridian across the joint. The localized high stresses generally develop within a narrow region enclosing the joint and may significantly affect the response behavior. Although for the preliminary design purpose, the structural response of the individual components may be examined. However, for the prediction of global behavior and rigorous optimal design, it may be more appropriate to analyze the joined complete shell system.

The buckling analysis of joined conical–cylindrical shells made up of isotropic materials has received the attention of many researchers. The elastic buckling and post-buckling analyses of cone–cylinder and sphere–cylinder joined shells subjected to external pressure are investigated by Flores and Godoy (1991) using an axisymmetric finite element approach. It is brought out that the bifurcation loads of the complex shells are lower than those of the individual components, but the curvature of the unstable post-buckling path of the complex shells is less than that of the individual components indicating the lesser imperfection sensitivity of former compared to later. The elastic buckling/post-buckling ensuing due to the circumferential compressive membrane stress near the intersection of the large end of cone and cylinder subjected to internal pressure is also investigated (Teng, 1994, 1995, 1996; Teng and Ma, 1999; Zhao and Teng, 2003). The insertion of a toroidal segment between the cone and cylinder results in slightly higher external buckling pressures than that of cone–cylinder shell without transition (Anwen, 1998).

The advances in composite technology have lead to the application of laminated composite structural elements like cylindrical and conical shells, as stand alone components or joined together, as load bearing members in the design of more and more sophisticated futuristic structures. These structures are often expected to operate at elevated temperatures in many applications such as supersonic and hypersonic vehicles, rockets, satellites, and nuclear components. The temperature rise due to boundary restraints may introduce compressive membrane state of stress leading to thermo-elastic instabilities/buckling failures. The studies on the thermo-elastic buckling analyses of axisymmetric shell geometries are limited to individual conical or cylindrical shells as evident from the review articles (Noor and Burton, 1992; Thornton, 1993; Argyris and Tenek, 1997) and from the brief literature review made in the recent studies on thermo-elastic buckling of shells Patel et al. (2004, 2005, in press). In order to optimally exploit the strength and load carrying capacity of laminated composite joined conical–cylindrical shells at elevated temperatures, accurate prediction and understanding of their thermal buckling/post-buckling characteristics is important. However, to the best of the authors' knowledge, there are no studies available on the thermo-elastic buckling/post-buckling characteristics of joined conical–cylindrical shells.

Therefore, in the present work, the thermo-elastic buckling/post-buckling characteristics of laminated joined circular conical–cylindrical shells subjected to uniform temperature rise are studied through nonlinear static analysis employing semi-analytical finite element approach Patel et al. (2005, in press). Geometric nonlinearity is introduced in the formulation using von Karman's strain-displacement relations. The presence of asymmetric perturbation in the form of small magnitude load spatially proportional to the linear buckling mode shape is assumed to initiate the bifurcation of the shell deformation from axisymmetric mode to asymmetric one. The study is carried out to highlight the influences of semi-cone angle, material properties and number of circumferential waves on the nonlinear thermo-elastic response of the different configurations of joined circular conical–cylindrical laminated shells.

2. Formulation

An axisymmetric laminated composite shell of revolution is considered with the coordinates s, θ and z along the meridional, circumferential and radial/thickness directions, respectively. The displacements u, v, w at a point (s, θ, z) from the median surface are expressed as functions of middle-surface displacements u_o, v_0 and w_0, and independent rotations β_s and β_θ of the meridional and hoop sections, respectively, as

$$
\begin{aligned}
u(s,\theta,z) &= u_0(s,\theta) + z\beta_s(s,\theta)\\
v(s,\theta,z) &= v_0(s,\theta) + z\beta_\theta(s,\theta)\\
w(s,\theta,z) &= w_0(s,\theta)
\end{aligned}
\tag{1}
$$

Using the semi-analytical approach, u_0, v_0, w_0, β_s and β_θ are represented by a Fourier series in the circumferential angle θ. For the nth harmonic, these can be written as

$$
\begin{aligned}
u_0(s,\theta) &= u_0^o(s) + \sum_{i=1}^{2}\left[u_0^{c_i}(s)\cos(in\theta) + u_0^{s_i}(s)\sin(in\theta)\right]\\
v_0(s,\theta) &= v_0^o(s) + \sum_{i=1}^{2}\left[v_0^{c_i}(s)\cos(in\theta) + v_0^{s_i}(s)\sin(in\theta)\right]\\
w_0(s,\theta) &= w_0^o(s) + \sum_{i=1}^{2}\left[w_0^{c_i}(s)\cos(in\theta) + w_0^{s_i}(s)\sin(in\theta)\right]\\
\beta_s(s,\theta) &= \beta_s^o(s) + \sum_{i=1}^{2}\left[\beta_s^{c_i}(s)\cos(in\theta) + \beta_s^{s_i}(s)\sin(in\theta)\right]\\
\beta_\theta(s,\theta) &= \beta_\theta^o(s) + \sum_{i=1}^{2}\left[\beta_\theta^{c_i}(s)\cos(in\theta) + \beta_\theta^{s_i}(s)\sin(in\theta)\right]
\end{aligned}
\tag{2}
$$

where superscript o refers to the axisymmetric component of displacement field variables, and c_i and s_i refer to the asymmetric components of the field variables having circumferential variation proportional to $\cos(in\theta)$ and $\sin(in\theta)$, respectively.

The above displacement variations in the circumferential direction are chosen according to the physics of the large deformation of shells of revolution i.e., participation of axisymmetric mode and higher asymmetric modes (Amabili et al., 1999; Patel et al., 2003; Tong and Pian, 1974; Ueda, 1979).

Using von Karman's assumption for moderately large deformation, Green's strains can be written in terms of mid-plane deformations as

$$
\{\varepsilon\} = \begin{Bmatrix} \varepsilon_p^{\mathrm{L}} \\ 0 \end{Bmatrix} + \begin{Bmatrix} z\varepsilon_{\mathrm{b}} \\ \varepsilon_{\mathrm{s}} \end{Bmatrix} + \begin{Bmatrix} \varepsilon_p^{\mathrm{NL}} \\ 0 \end{Bmatrix}
\tag{3}
$$

The membrane $\{\varepsilon_p^{\mathrm{L}}\}$, bending $\{\varepsilon_{\mathrm{b}}\}$, shear $\{\varepsilon_{\mathrm{s}}\}$ and nonlinear in-plane $\{\varepsilon_p^{\mathrm{NL}}\}$ strains in Eq. (3) are written as (Kraus, 1976)

$$
\left\{\varepsilon_p^{\mathrm{L}}\right\} = \begin{Bmatrix} \dfrac{\partial u_0}{\partial s} + \dfrac{w_0}{R} \\ \dfrac{u_0\sin\phi}{r} + \dfrac{\partial v_0}{r\partial\theta} + \dfrac{w_0\cos\phi}{r} \\ \dfrac{\partial u_0}{r\partial\theta} - \dfrac{v_0\sin\phi}{r} + \dfrac{\partial v_0}{\partial s} \end{Bmatrix}; \quad \{\varepsilon_{\mathrm{b}}\} = \begin{Bmatrix} \dfrac{\partial\beta_{\mathrm{s}}}{\partial s} + \dfrac{\partial u_0}{R\partial s} \\ \dfrac{\beta_{\mathrm{s}}\sin\phi}{r} + \dfrac{\partial\beta_\theta}{r\partial\theta} + \dfrac{u_0\sin\phi}{Rr} \\ \dfrac{1}{R}\dfrac{\partial u_0}{r\partial\theta} + \dfrac{\partial v_0}{\partial s}\dfrac{\cos\phi}{r} + \dfrac{\partial\beta_{\mathrm{s}}}{r\partial\theta} + \dfrac{\partial\beta_\theta}{\partial s} - \dfrac{\beta_\theta\sin\phi}{r} \end{Bmatrix};
$$

$$
\{\varepsilon_{\mathrm{s}}\} = \begin{Bmatrix} \beta_{\mathrm{s}} + \dfrac{\partial w_0}{\partial s} \\ \beta_\theta + \dfrac{\partial w_0}{r\partial\theta} - \dfrac{v_0\cos\phi}{r} \end{Bmatrix}; \quad \left\{\varepsilon_p^{\mathrm{NL}}\right\} = \begin{Bmatrix} \dfrac{1}{2}\left(\dfrac{\partial w_0}{\partial s}\right)^2 \\ \dfrac{1}{2}\left(\dfrac{\partial w_0}{r\partial\theta}\right)^2 \\ \dfrac{\partial w_0}{\partial s}\dfrac{\partial w_0}{r\partial\theta} \end{Bmatrix}
\tag{4}
$$

where r, R and ϕ are the radius of the parallel circle, radius of the meridional circle and angle made by the tangent at any point in the shell with the axis of revolution, respectively.

The minimization of total potential energy functional consisting of strain energy, potential of transverse load and initial state of stress, leads to the governing equation for the deformation of the shell as

$$[[\boldsymbol{K}] - [\boldsymbol{K}_{\mathrm{T}}] + [\boldsymbol{K}_{\mathrm{G}}] + (1/2)[\boldsymbol{N}_1(\boldsymbol{\delta})] + (1/3)[\boldsymbol{N}_2(\boldsymbol{\delta})]]\{\boldsymbol{\delta}\} = \{\boldsymbol{F}_{\mathrm{M}}\} + \{\boldsymbol{F}_{\mathrm{T}}\} \tag{5}$$

where $[\boldsymbol{K}]$ is the linear stiffness matrix, $[\boldsymbol{N}_1]$ and $[\boldsymbol{N}_2]$ are nonlinear stiffness matrices linearly and quadratically dependent on the field variables, respectively. $[\boldsymbol{K}_{\mathrm{T}}]$ and $[\boldsymbol{K}_{\mathrm{G}}]$ are the geometric stiffness matrices due to thermal and initial stress resultants. $\{\boldsymbol{F}_{\mathrm{M}}\}$ and $\{\boldsymbol{F}_{\mathrm{T}}\}$ are mechanical and thermal load vectors.

The governing Eq. (5) can be employed to study the linear/nonlinear static and eigenvalue buckling analyses by neglecting the appropriate terms as:

Linear static analysis:

$$[\boldsymbol{K}]\{\boldsymbol{\delta}\} = \{\boldsymbol{F}_{\mathrm{M}}\} + \{\boldsymbol{F}_{\mathrm{T}}\} \tag{6}$$

Nonlinear static analysis:

$$[[\boldsymbol{K}] - [\boldsymbol{K}_{\mathrm{T}}] + (1/2)[\boldsymbol{N}_1(\boldsymbol{\delta})] + (1/3)[\boldsymbol{N}_2(\boldsymbol{\delta})]]\{\boldsymbol{\delta}\} = \{\boldsymbol{F}_{\mathrm{M}}\} + \{\boldsymbol{F}_{\mathrm{T}}\} \tag{7}$$

Eigenvalue buckling analysis:

$$[\boldsymbol{K}]\{\boldsymbol{\delta}\} = \Delta T[\boldsymbol{K}^*_{\mathrm{G}}]\{\boldsymbol{\delta}\} \tag{8}$$

where $[\boldsymbol{K}^*_{\mathrm{G}}]$ is the geometric stiffness due initial state of stress developed because of unit uniform temperature rise and ΔT is the temperature rise.

It may be noted here that for the purpose of evaluating $[\boldsymbol{K}^*_{\mathrm{G}}]$, firstly the static analysis of the shell using Eq. (6) for unit temperature rise is carried out. The resulting deformation filed is used to calculate the initial state of stress resultants used in evaluating the $[\boldsymbol{K}^*_{\mathrm{G}}]$ matrix.

The nonlinear pre-buckling followed by post-buckling equilibrium path is traced by solving Eq. (7) using Newton–Raphson iteration procedure coupled with displacement control method (Batoz and Dhatt, 1979). The degree of freedom that has the highest increment in the previous step is selected as a control parameter. The equilibrium iterations are continued for each load/displacement incremental step until the convergence criteria suggested by Bergan and Clough (1972) are satisfied within the specific tolerance limit of less than 0.01%.

The detailed description of finite element formulation and its validation for thermo-elastic buckling/post-buckling studies of laminated conical and cylindrical shells can be found in Patel et al. (2005, in press) and are not presented here for the sake of brevity.

3. Results and discussion

Here, mainly the thermo-elastic nonlinear pre-buckling path followed by post-buckling characteristics of laminated joined circular conical–cylindrical and conical–cylindrical–conical shells (Fig. 1) subjected to uniform temperature rise are investigated using the semi-analytical finite element formulation. The study is carried out to highlight the influences of semi-cone angle (ϕ), material properties and number of circumferential waves (n) on the nonlinear pre-buckling/post-buckling response described as maximum outward normal displacement parameter ($w_{\max}/h$; h is the total thickness of the shell) versus temperature parameter $T(=\Delta T\alpha_0 r_2/h$; $\alpha_o = 10^{-6}/^{\circ}\mathrm{C}$ and ΔT is the temperature rise) curves for the laminated joined shells.

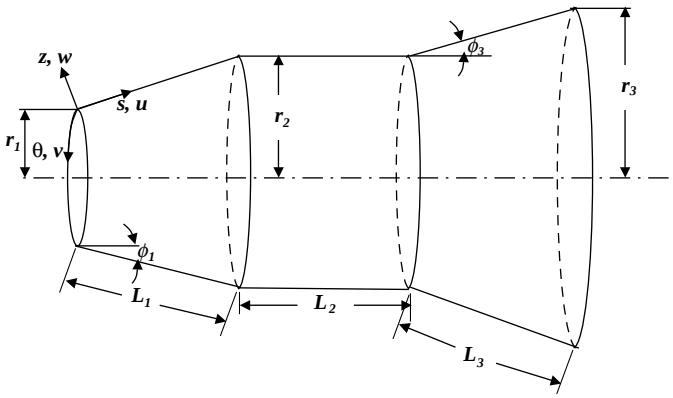

Fig. 1. Coordinate system and geometrical details of conical–cylindrical–conical shell.

The material properties used for the detailed studies are

Material 1

$$E_{\mathrm{L}}/E_{\mathrm{T}} = 10.8, \quad G_{\mathrm{LT}}E_{\mathrm{T}} = G_{\mathrm{TT}}/E_{\mathrm{T}} = 0.71, \quad \nu_{\mathrm{LT}} = \nu_{\mathrm{TT}} = 0.28, \quad \alpha_{\mathrm{T}}/\alpha_{\mathrm{L}} = 1125 \text{ or } 10$$

where E, G, ν and α are Young's modulus, shear modulus, Poisson's ratio and coefficient of thermal expansion, respectively. The subscripts L and T are the longitudinal and transverse directions respectively with respect to the fibers.

Material 2

$$E_{\mathrm{L}}/E_{\mathrm{T}} = 25, \quad G_{\mathrm{LT}}/E_{\mathrm{T}} = 0.5, \quad G_{\mathrm{TT}}/E_{\mathrm{T}} = 0.2, \quad \nu_{\mathrm{LT}} = \nu_{\mathrm{TT}} = 0.25, \quad \alpha_{\mathrm{T}}/\alpha_{L} = 10$$

All the layers are of equal thickness and the ply-angle is measured with respect to the meridional axis (s-axis). The first layer is the innermost layer of the shell.

The details of simply supported immovable boundary conditions at the two ends of joined shell system considered here are

$$u_0^o = u_0^{c1} = u_0^{s1} = u_0^{c2} = u_0^{s2} = v_0^o = v_0^{c1} = v_0^{s1} = v_0^{c2} = v_0^{s2} = 0$$
$$w_0^o = w_0^{c1} = w_0^{s1} = w_0^{c2} = w_0^{s2} = \beta_\theta^o = \beta_\theta^{c1} = \beta_\theta^{s1} = \beta_\theta^{c2} = \beta_\theta^{s2} = 0 \qquad \text{at } s = 0, L$$

where $L(= L_1 + L_2 + L_3)$ is the total meridional length of the joined shell.

Based on progressive mesh refinement, 48 elements idealization (16 elements in each segment) is found to be adequate to model the complete length of the joined conical–cylindrical–conical shell system.

Before proceeding for the detailed nonlinear buckling/post-buckling analysis, the distribution of in-plane stress resultants $[(N_{ss}, N_{\theta\theta}) = \sum_{k=1}^{N} \int_{h_k}^{h_{k+1}} (\sigma_{ss}^o, \sigma_{\theta\theta}^o)\,\mathrm{d}z]$ is evaluated through linear static analysis to investigate the influence of joints between conical and cylindrical shells on the distribution of thermal stress resultants. The results for the eight-layered cross-ply $(0°/90°)_4$ conical–cylindrical and conical–cylindrical–conical thin shells ($r_2/h = 200$, $L_2/r_2 = 1$, $L_1 = L_2 = L_3$, Material 1: $\alpha_T\,\alpha_{\mathrm{L}} = 1125$) subjected to uniform temperature rise ($\Delta T = 1$) are highlighted in Fig. 2. It can be observed from this figure that the meridional stress resultant (N_{ss}) is uniform in the cylindrical section whereas it shows decreasing magnitude trend from smaller diameter end to larger diameter end of the conical section. The magnitude of N_{ss} in the cylindrical portion of the joined shell decreases with the increase in the semi-cone angle of the conical section. The rate of

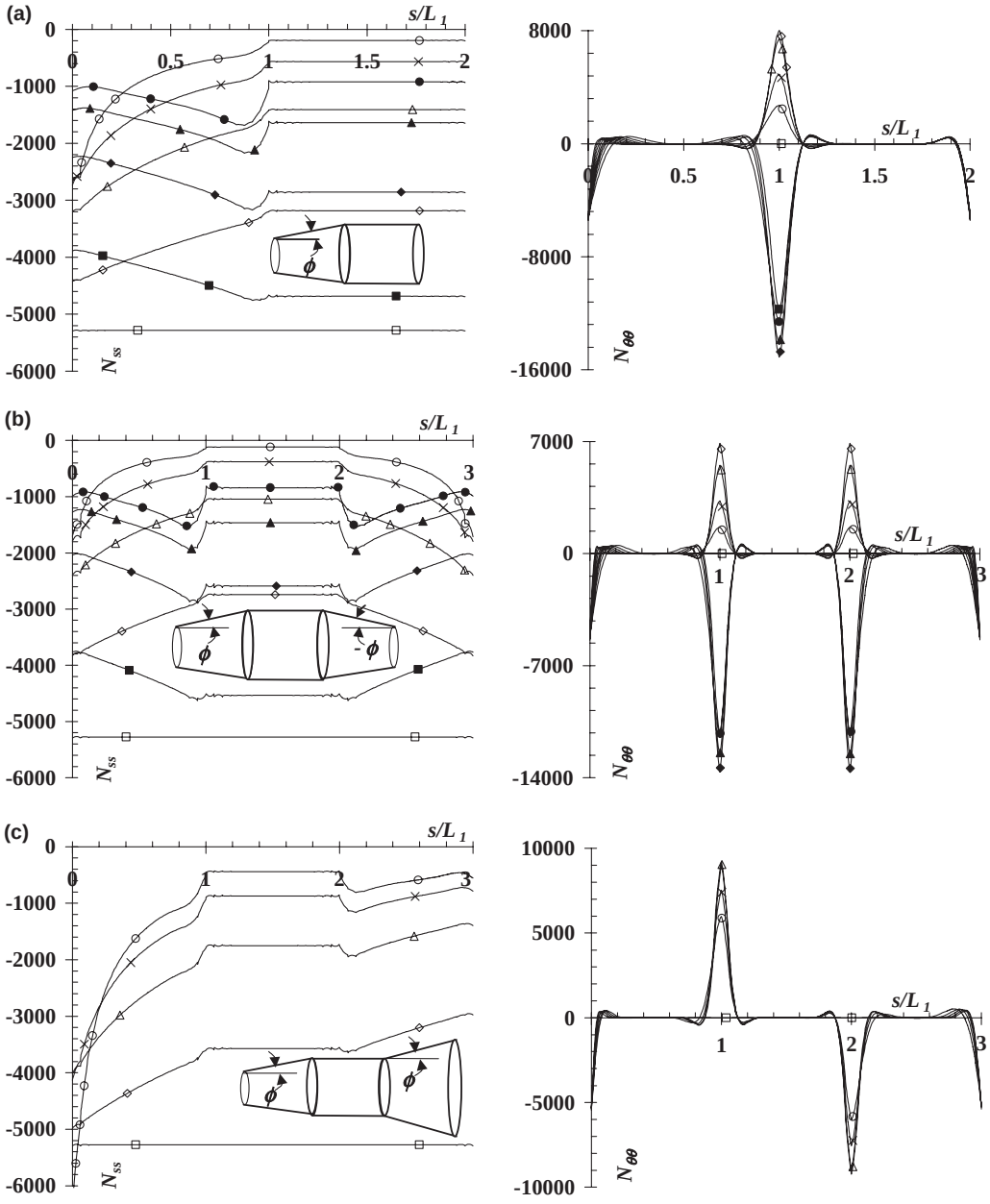

Fig. 2. Distribution of meridional (N_{ss}) and hoop ($N_{\theta\theta}$) stress resultants along meridional direction (s) ((□) $\phi = 0°$, (◊) 15°, (△) 30°, (×) 45°, (○) 60°, (■) −15°, (♦) −30°, ▲ −45°, ● −60°): (a) Cone–cylinder, (b) cone–cylinder–cone-I ($\phi_1 = -\phi_3 = \phi$) (c) Cone–cylinder–cone-II ($\phi_1 = \phi_3 = \phi$).

change of N_{ss} along meridional direction in the conical section near the joints is significantly higher. For certain shell combinations, the meridional stress resultant rises sharply to significantly higher values near smaller diameter edge of shallow conical section cases (Fig. 2(c)). The presence of the hoop stress resultant

($N_{\theta\theta}$) is predicted near the joints and supports of the shell system. The nature of the $N_{\theta\theta}$ is compressive near the supports irrespective of the shell configurations whereas near the joints it depends on the cone angle. The compressive nature of the hoop stress resultant is observed near the joint between the smaller end of the cone and cylinder whereas the tensile nature around the joint between larger diameter end of the cone

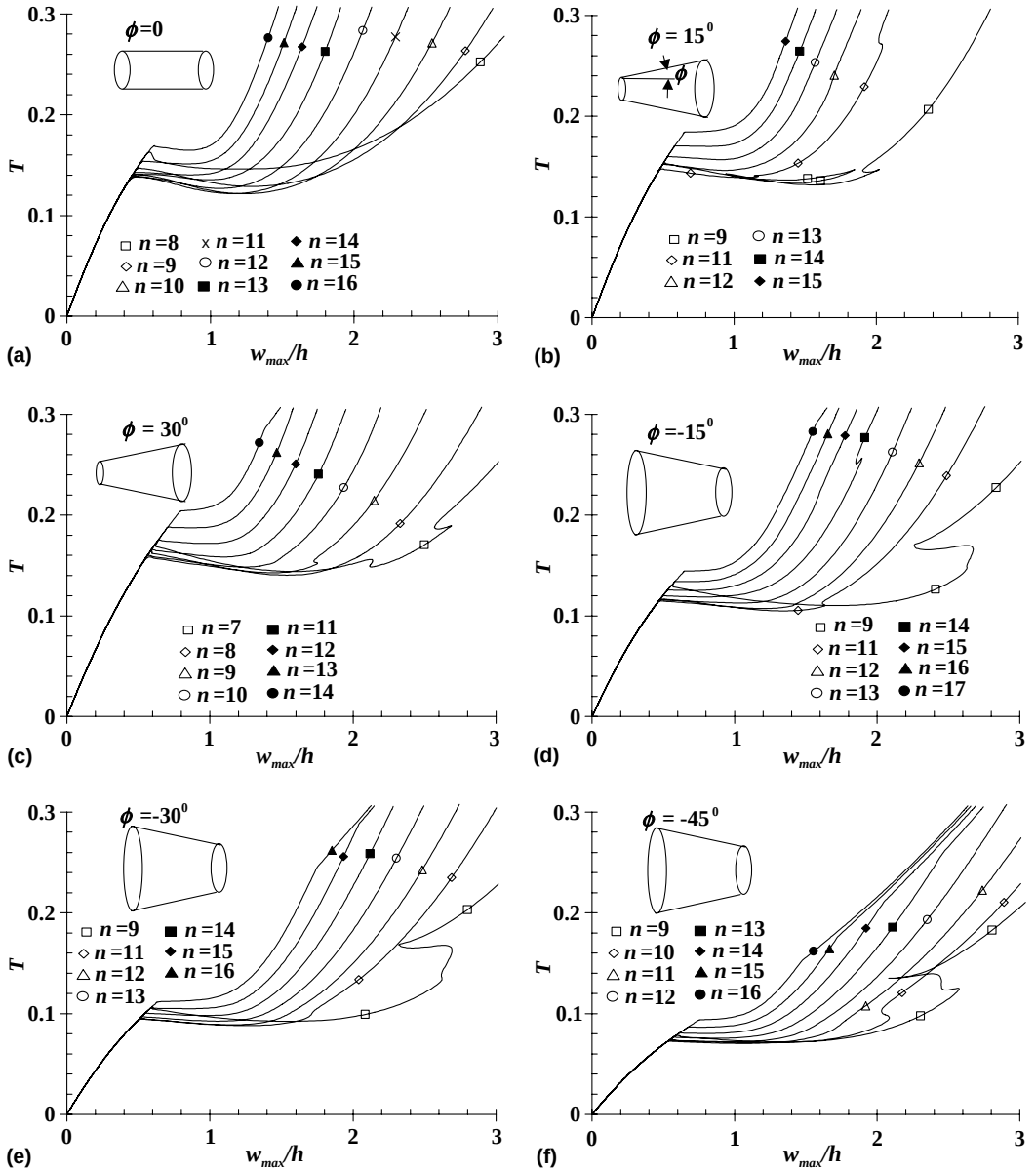

Fig. 3. Maximum displacement ($w_{\max}/h$) versus temperature parameter (T) curves for cross-ply laminated circular conical shells (Material 1): (a) $\phi = 0°$; (b) $\phi = 15°$; (c) $\phi = 30°$; (d) $\phi = -15°$; (e) $\phi = -30°$; (f) $\phi = -45°$.

and cylinder. The stress field predicted in the static analysis is employed for evaluating the geometric matrix and in turn for the linear eigenvalue buckling analysis.

Next, the nonlinear thermo-elastic response characteristics of cross-ply laminated eight layered $(0°/90°)_4$ conical shells ($r_2/h = 200$, $L_1/r_2 = 1$, Material 1: $\alpha_T/\alpha_L = 1125$) with different semi-cone angles ($\phi = 0°, 15°, 30°, -15°, -30°, -45°$) are highlighted in Fig. 3 considering different circumferential wave numbers (n) of asymmetric perturbation in the form of small magnitude load spatially proportional to the linear buckling mode shapes. It can be viewed from this figure that the pre-buckling deformation path of the shells is independent of the circumferential wave number of the small magnitude perturbation distribution. The critical temperature corresponding to the bifurcation of equilibrium path from primary one with axisymmetric circumferential displacement distribution to secondary asymmetric one depends on the circumferential wave number (n). The bifurcation temperature increases for diverging conical shells and decreases for the converging conical shells while increasing the semi-cone angle with fixed right edge radius (r_2). It can also be noticed from Fig. 3 that the bifurcation temperature for a particular shell initially increases with circumferential wave number (n), attains a minimum value and then again increases with the increase in the wave number (n). Thus there exists a critical circumferential wave number (n_{cr}) leading to minimum bifurcation temperature. However, in the post-buckling region at a particular temperature level, the maximum displacement reduces with the increase in circumferential wave number monotonically. The post-buckling response immediately after the bifurcation is of snap-through type for lower circumferential wave numbers and of stable type for higher wave numbers (n). The comparison of bifurcation temperature parameter predicted based linear eigenvalue and nonlinear analyses is made and given in Table 1. It can be seen from this table that the eigenvalue analysis underestimates the bifurcation temperature compared to that evaluated from nonlinear analysis. However, the circumferential wave number corresponding to lowest bifurcation temperature is same from both the analyses.

Next, the nonlinear pre- and post-buckling characteristics of different shell combinations ($r_2/h = 200$, $L_2/r_2 = 1$, $L_1 = L_2 = L_3$; $(0°/90°)_4$) are studied and the results for semi-cone angle magnitudes of 15° and 30° are highlighted in Figs. 4 and 5, respectively, together with those of individual cylinder and conical shells for comparison purpose. It is observed from these figures that the critical bifurcation temperature of the joined shell system compared to the individual shells is higher and this difference increases with the increase in the magnitude of the semi-cone angle (ϕ). This may be attributed to the more relative reduction in the meridional thermal stress resultant compared to the decrease in the stiffness due to the increase in

Table 1
Comparison of bifurcation temperature parameter evaluated from linear eigenvalue (T_{crL}) and nonlinear static (T_{crNL}) analyses for different values of semi-cone angle (ϕ) and circumferential wave number (n)

n	Semi-cone angle (ϕ)											
	0°		15°		30°		−15°		−30°		−45°	
	T_{crL}[a]	T_{crNL}[b]	T_{crL}	T_{crNL}	T_{crL}	T_{crNL}	T_{crL}	T_{crNL}	T_{crL}	T_{crNL}	T_{crL}	T_{crNL}
8	0.162	0.163	0.160	0.166	0.154	0.164	0.141	0.147	0.112	0.120	0.079	0.085
9	0.144	0.147	0.148	0.154	0.153	0.158	0.126	0.131	0.101	0.107	0.073	0.078
10	0.133	0.141	0.142	0.148	0.155	0.160	0.116	0.122	0.094	0.099	0.069	0.074
11	0.127	0.139	0.142	0.148	0.157	0.166	0.111	0.117	0.090	0.095	0.068	0.073
12	0.126	0.138	0.145	0.152	0.163	0.175	0.109	0.115	0.090	0.095	0.069	0.074
13	0.129	0.141	0.149	0.160	0.171	0.188	0.109	0.116	0.091	0.097	0.070	0.077
14	0.134	0.143	0.157	0.169	0.181	0.204	0.112	0.120	0.092	0.100	0.073	0.081

[a] Linear eigenvalue analysis.
[b] Nonlinear static analysis.

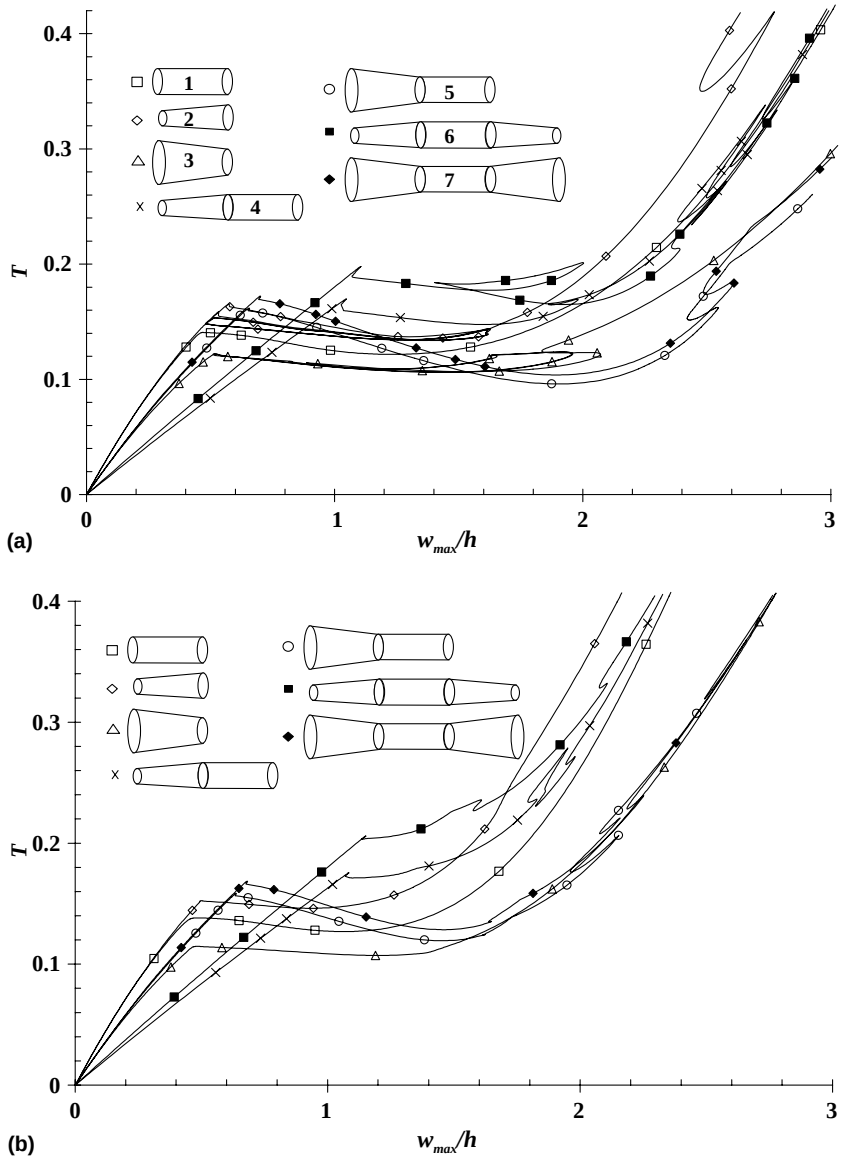

Fig. 4. Maximum displacement (w_{max}/h) versus temperature parameter (T) curves for cross-ply laminated shells with different configurations (Material 1: $\alpha_T/\alpha_L = 1125$, $\phi = 15°$) (a) $n = 10$, (b) $n = 12$.

the effective length of the joined shells. This behavior is unlike the characteristics of joined shells subjected to external pressure wherein the pre-buckling stress distribution is same as that in the individual components (except very near to the joint) and hence the decrease in the stiffness leads to the decrease in critical bifurcation pressure of joined shells (Flores and Godoy, 1991). The post-buckling response of shell combination may differ considerably compared to individual shells depending upon the temperature/displacement level. The degree of snap-through is significantly higher when the cylindrical section is joined with smaller edge of the conical sections. For certain shell system parameters and temperature/displacement level, the

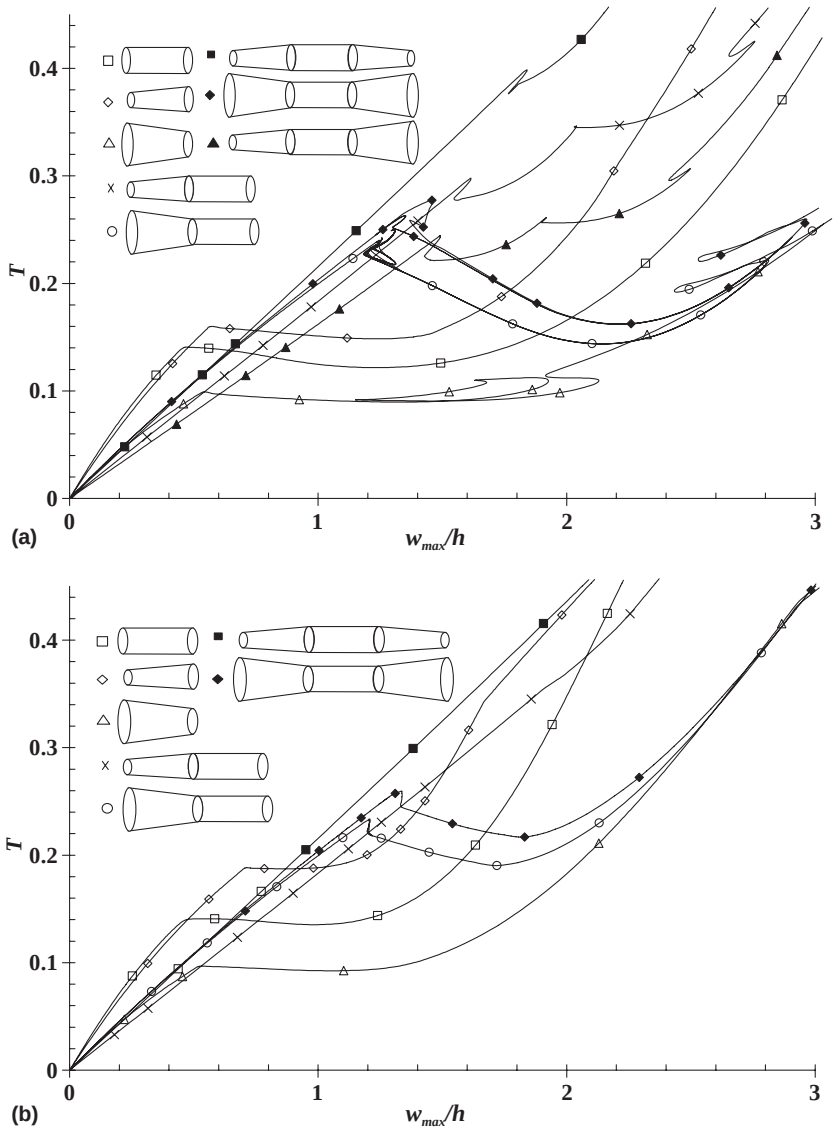

Fig. 5. Maximum displacement ($w_{\max}/h$) versus temperature parameter (T) curves for cross-ply laminated shells with different configurations (Material 1: $\alpha_T/\alpha_L = 1125$, $\phi = 30°$) (a) $n = 10$, (b) $n = 13$.

post-buckling equilibrium path is not unique and there exists multiple post-buckling equilibrium configurations. The bifurcation temperature parameter evaluated from linear eigenvalue and nonlinear analyses are given in Table 2 for different shell configurations as indicated in the inserted diagrams in Fig. 4(a). It can be seen from this table that the linear eigenvalue overestimates the critical temperature parameter compared to that from nonlinear analysis for shell combinations having joint between larger edge side of the conical-section and cylinder whereas for other cases eigenvalue analysis under predicts the critical temperature parameter values.

Table 2
Comparison of bifurcation temperature parameter evaluated from linear eigenvalue (T_{crL}) and nonlinear static (T_{crNL}) analyses for different shell configurations shown as inserted diagrams in Fig. 4(a)

Shell configuration number	Semi-cone angle (ϕ) = 15°				$\phi = 30°$			
	Circumferential wave number (n) = 10		$n = 12$		$n = 10$		$n = 13$	
	T_{crL}[a]	T_{crNL}[b]	T_{crL}	T_{crNL}	T_{crL}	T_{crNL}	T_{crL}	T_{crNL}
1	0.133	0.141	0.126	0.138	0.133	0.141	0.129	0.141
2	0.142	0.148	0.145	0.152	0.155	0.160	0.171	0.188
3	0.116	0.122	0.109	0.115	0.094	0.099	0.091	0.097
4	0.199	0.170	0.202	0.176	0.356	0.298	0.412	–
5	0.123	0.162	0.111	0.158	0.146	0.239	0.122	0.233
6	0.231	0.198	0.235	0.206	0.479	0.399	0.554	–
7	0.128	0.172	0.115	0.169	0.161	0.263	0.135	0.259

[a] Linear eigenvalue analysis.
[b] Nonlinear static analysis.

The evolution of post-buckling deformation shapes for the conical–cylindrical and conical–cylindrical–conical joined shell configurations considered in Fig. 4(a) is highlighted in Figs. 6–9. In these figures the post-buckling deformation shapes corresponding to the points marked (b, c, d,...) in temperature parameter (T) versus maximum displacement (w_{max}/h) curves are shown considering full meridional length and partial circumferential length ($\theta = 0$ to $2\pi/n$). It can be seen from Figs. 6–9 that the post bifurcation deformation pattern changes significantly along the equilibrium. It can further be inferred from these figures that the conversion of membrane energy to bending energy starts near the joint and then progresses in the full shell with increase in temperature/maximum displacement depending upon the shell parameters.

The influence of semi-cone angle on the pre- and post-buckling behavior of cone–cylinder and cone–cylinder–cone shell combinations together with the effect of thermal expansion coefficient ratio (α_T/α_L) is studied and the results pertaining to circumferential wave number associated with the lowest critical temperature in the eigenvalue analysis are depicted in Fig. 10. It can be observed from this figure that the pre-buckling stiffness decreases with the increase in the magnitude of the negative semi-cone angle of the shells whereas it increases with the increase in the positive semi-cone angle and general trend of shells with decreasing pre-buckling stiffness in terms of semi-cone angle is: $0° > 60° > -15° > 45° > -30° > 30° > 15° > -45° > -60°$. It can also be observed from this figure that the certain shell combinations such as cylinder with $-15°$ conical-section and cylinder with 45° conical-section yield very close pre-buckling equilibrium path. The combined influence of the shell stiffness and the membrane stress distribution leads to the increasing critical bifurcation temperature with the increase in the magnitude of the semi-cone angle. It is also revealed from this figure that the shell combinations with higher semi-cone angle magnitude do not undergo bifurcation buckling. It can further be noticed from this figure that the relative post-buckling strength among the shell combinations with different semi-cone angles may change at higher displacement magnitudes. One can also infer from this figure that the two-section shells yield lowest bifurcation temperature and three-section shells with $\alpha_T/\alpha_L = 10$ highest critical temperature. The bifurcation temperature parameter evaluated from eigenvalue (T_{crL}) and nonlinear (T_{crNL}) analyses together with the lowest temperature parameter in the post-buckling path (T_{LP}) is presented in Table 3. It can be inferred from this table that there exists a lower temperature in the post-buckling path compared to bifurcation temperature predicted from nonlinear analysis for the shells considered in Fig. 6. Furthermore, the linear eigenvalue analysis highly under or over predicts the bifurcation temperature compared to that predicted from nonlinear analysis and the percentage difference between eigenvalue and nonlinear prediction of bifurcation

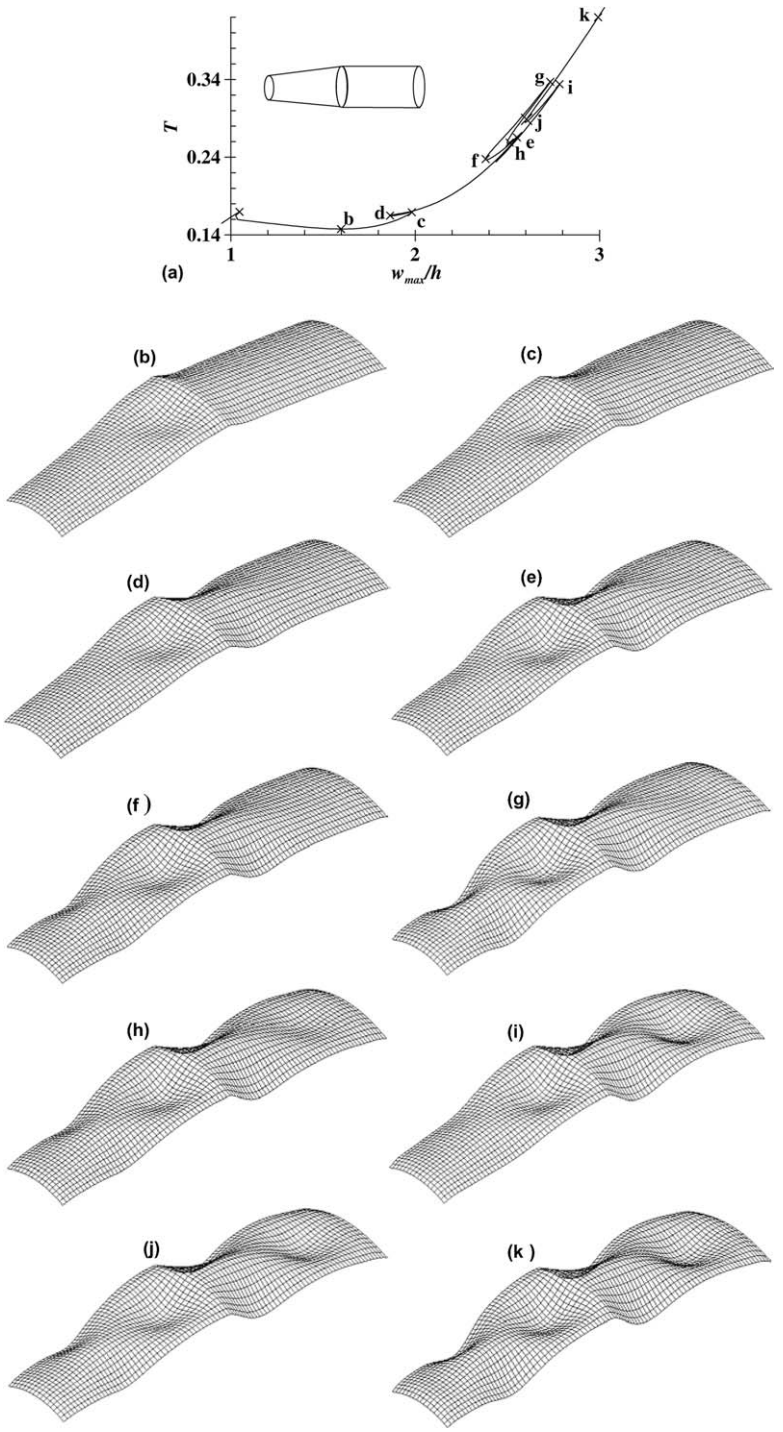

Fig. 6. Post-buckling deformation shapes of conical–cylindrical shell ($\phi_1 = 15°$) corresponding to the points marked in Fig. 6(a).

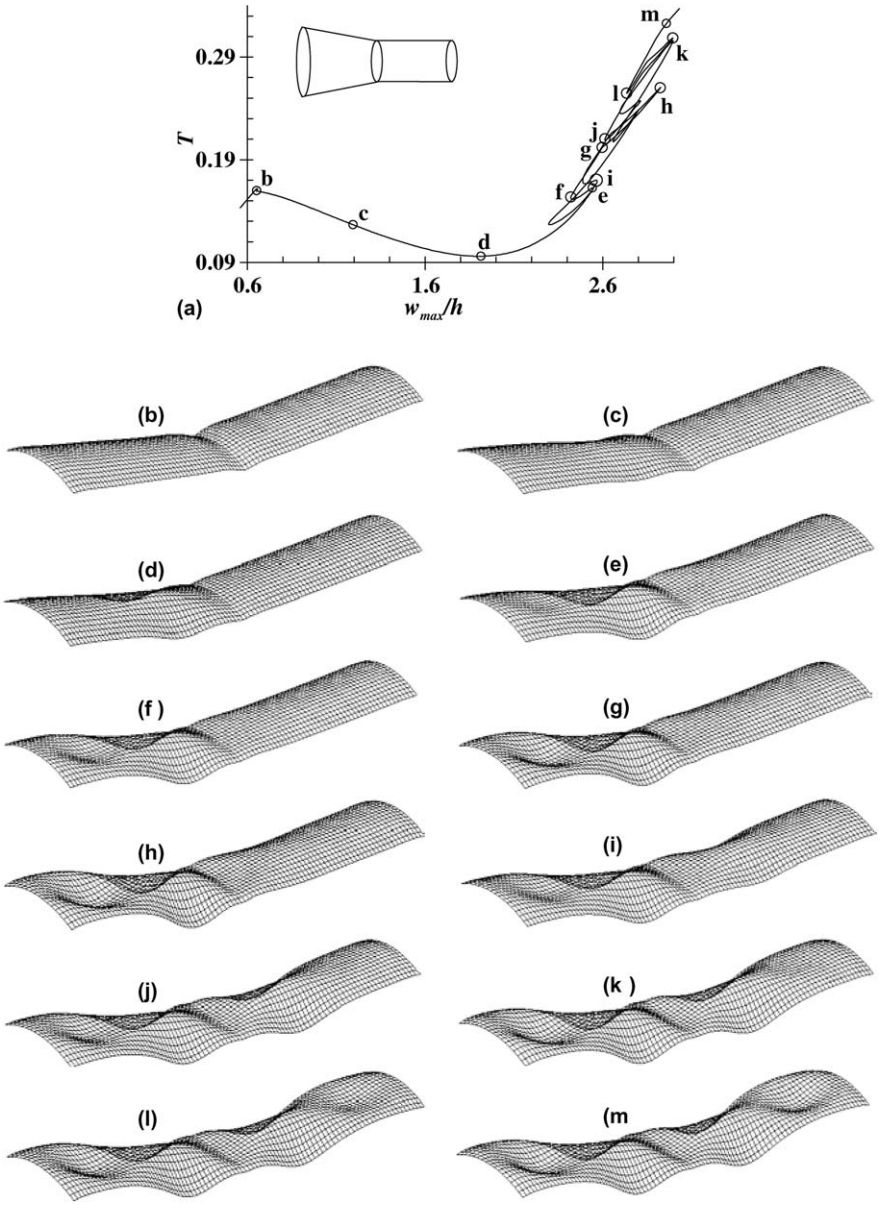

Fig. 7. Post-buckling deformation shapes of conical–cylindrical shell ($\phi_1 = -15°$) corresponding to the points marked in Fig. 7(a).

temperature increases with the increase in the semi-cone angle of the conical section of the joined shells.

The influence of circumferential wave number on the post-buckling characteristics of two-section conical–cylindrical shells is presented in Fig. 11 for different values of semi-cone angle. It can be viewed from this figure that the shells at lower circumferential wave numbers reveal snap-through type of post-buckling response whereas for higher wave numbers depending upon the semi-cone angle the shells may reveal stable

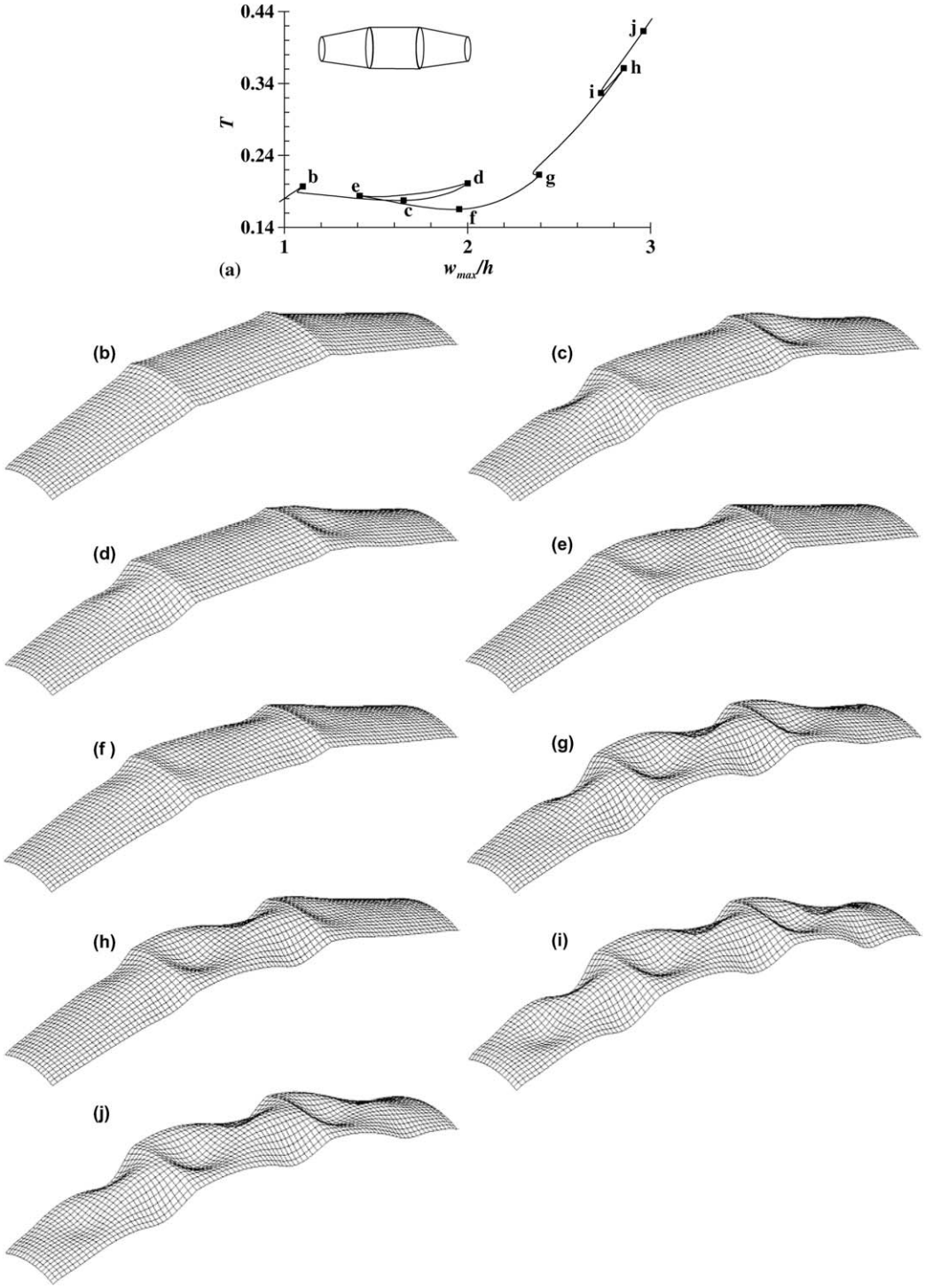

Fig. 8. Post-buckling deformation shapes of conical–cylindrical–conical shell ($\phi_1 = -\phi_3 = 15°$) corresponding to the points marked in Fig. 8(a).

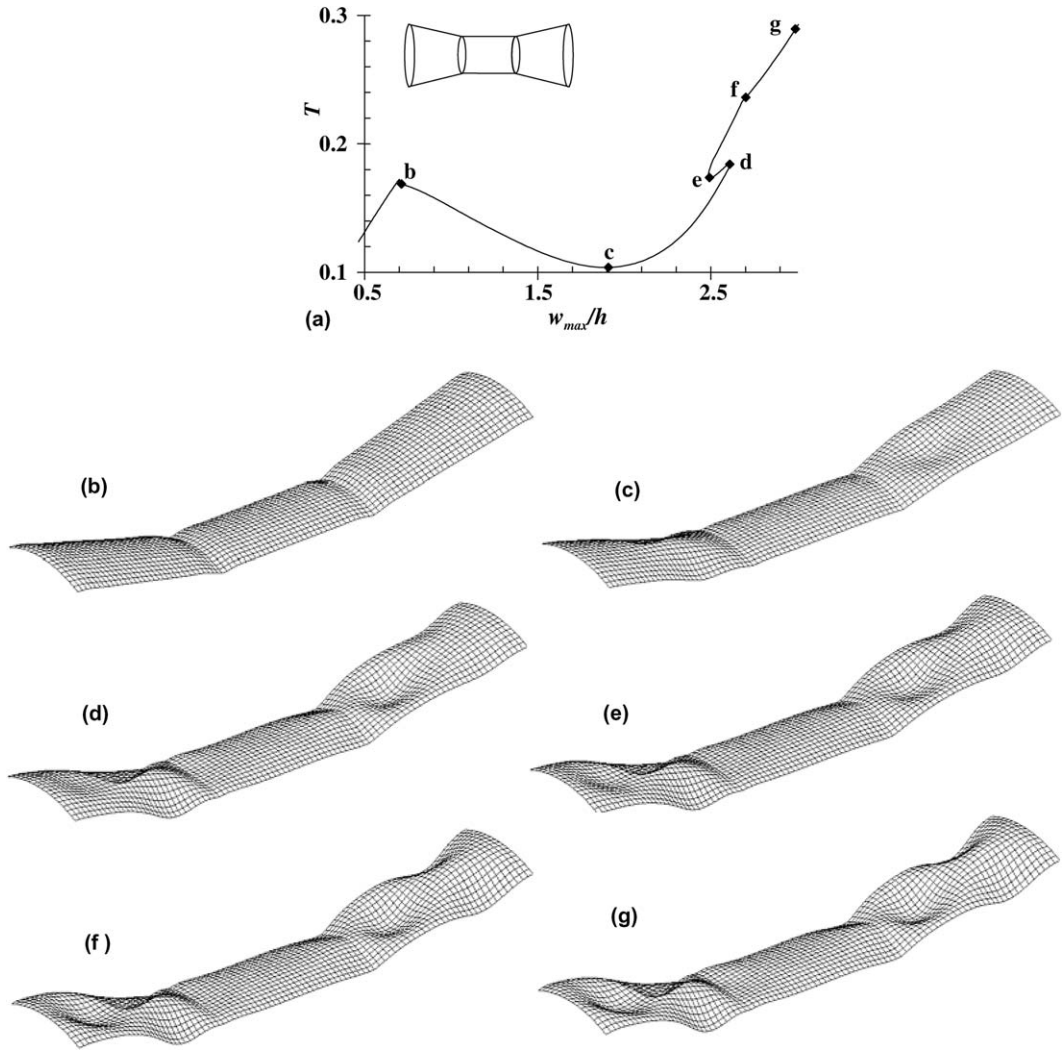

Fig. 9. Post-buckling deformation shapes of conical–cylindrical–conical shell ($-\phi_1 = \phi_3 = 15°$) corresponding to the points marked in Fig. 9(a).

post-buckling response. The existence of multiple equilibrium configurations in certain temperature range is also brought out specifically for semi-cone angle values of 15° and −15°.

To study the effect of material orthotropicity ratio (E_L/E_T) on the post-buckling response, the study is carried out for three section conical–cylindrical–conical shells with layers of Material 2 ($E_L/E_T = 25$). The pre- and post-buckling characteristics for different semi-cone angle values are presented in Fig. 12. It can be noticed from this figure that the post-buckling stiffness of the shells is very less and the deformation continues to grow without any further increase in temperature parameter even at higher displacement level ($w_{max}/h \geqslant 2$) specifically along the lowest post-buckling curves among different circumferential wave number (n).

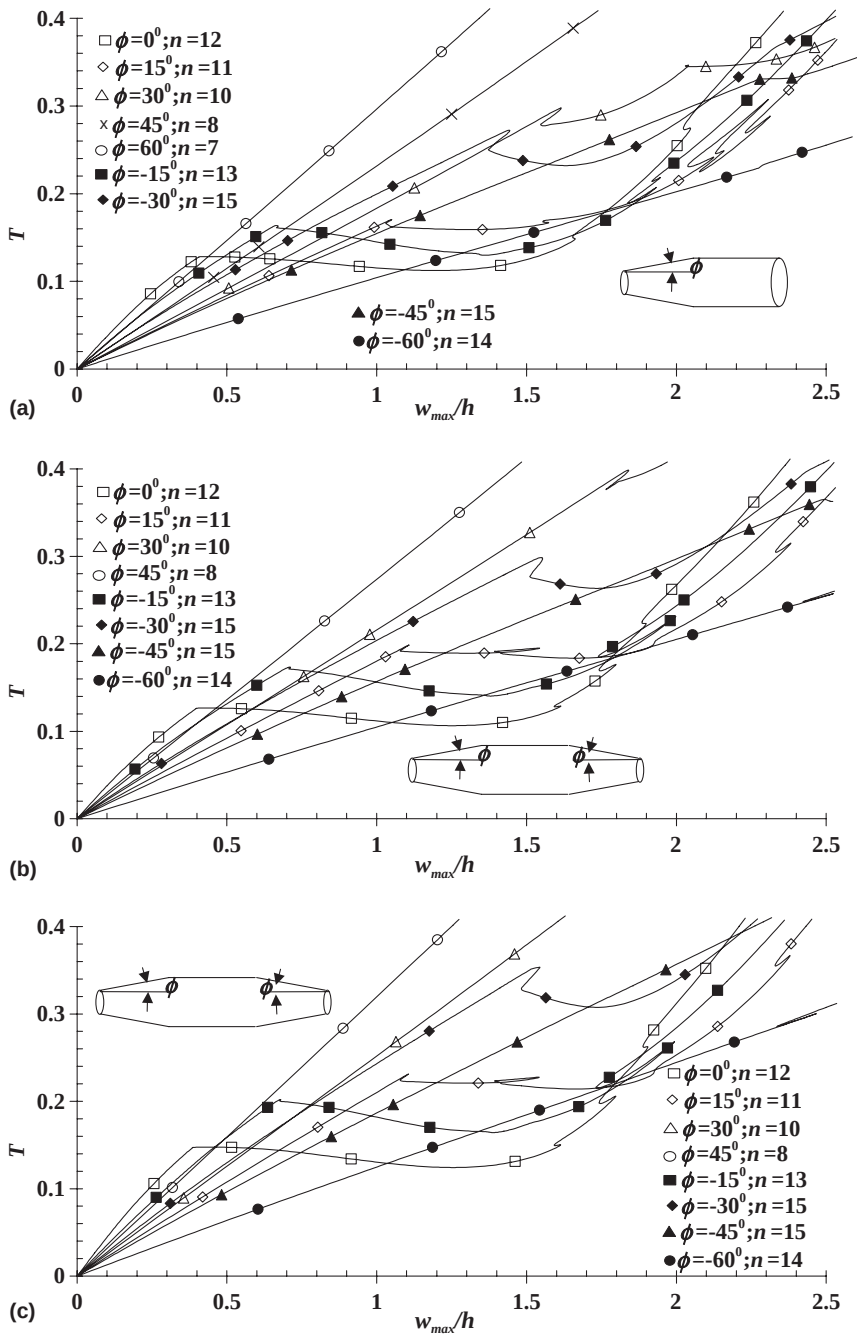

Fig. 10. Maximum displacement ($w_{\max}/h$) versus temperature parameter (T) curves for cross-ply laminated joined conical–cylindrical shells (Material 1): (a) cone–cylinder, $\alpha_T/\alpha_L = 1125$; (b) cone–cylinder–cone, $\alpha_T/\alpha_L = 1125$; (c) cone–cylinder–cone, $\alpha_T/\alpha_L = 10$.

Table 3
The bifurcation temperature parameter evaluated from linear eigenvalue (T_{crL}), nonlinear static (T_{crNL}) analyses and lowest temperature parameter (T_{LP}) in the post-buckling path for cone–cylinder and cone–cylinder–cone combinations with different values of semi-cone angle (ϕ) of conical section (Material 1)

Semi-cone angle (ϕ)	Cone–cylinder ($\alpha_T/\alpha_L = 1125$)			Cone–cylinder–cone ($\alpha_T/\alpha_L = 1125$)			Cone–cylinder–cone ($\alpha_T/\alpha_L = 10$)		
	T_{crL}	T_{crNL}	T_{LP}	T_{crL}	T_{crNL}	T_{LP}	T_{crL}	T_{crNL}	T_{LP}
0°	0.126	0.128	0.112	0.126	0.127	0.106	0.147	0.148	0.124
15°	0.197	0.170	0.159	0.229	0.198	0.184	0.266	0.231	0.221
30°	0.356	0.298	0.277	0.479	0.399	0.376	0.559	0.460	0.460
45°	0.581	0.464	0.408	0.869	0.686	0.609	1.013	0.796	0.707
−15°	0.109	0.164	0.130	0.113	0.173	0.140	0.132	0.202	0.164
−30°	0.119	0.272	0.232	0.132	0.299	0.263	0.154	0.354	0.308
−45°	0.127	0.332	0.329	0.142	0.365	0.363	0.166	0.434	0.431
−60°	0.114	0.234	0.234	0.126	0.261	0.248	0.147	0.300	0.286

4. Conclusions

The thermo-elastic buckling/post-buckling characteristics of laminated joined circular conical–cylindrical shells subjected to uniform temperature rise are analyzed here through nonlinear static analysis employing semi-analytical finite element approach. The study is carried out to highlight the influences of semi-cone angle, material properties and number of circumferential waves on the nonlinear thermo-elastic response of the different configurations of joined circular conical–cylindrical laminated shells. The following observations can be made from the detailed analysis carried out here:

(i) In the pre-buckling state, the uniform meridional stress resultant (N_{ss}) in the cylindrical section decreases in magnitude with the semi-cone angle of conical section and nonuniform N_{ss} distribution observed in the conical section shows decreasing magnitude trend from smaller diameter edge to larger diameter edge.
(ii) The pre-buckling hoop stress resultant ($N_{\theta\theta}$) is predicted near the joints and supports with compressive nature near the supports and compressive/tensile near the joint depending upon the cone angle.
(iii) The pre-buckling stiffness decreases with the increase in the magnitude of the negative semi-cone angle of the joined shells whereas it increases with the increase in the positive semi-cone angle although in either case it is lesser than corresponding cylindrical shell.
(iv) The critical bifurcation temperature of the joined shell system compared to the individual shells is higher and this difference increases with the increase in the magnitude of the semi-cone angle. The shell combinations with higher semi-cone angle magnitude may not even undergo bifurcation buckling.
(v) The joined shells may exhibit snap-through type or stable post-buckling response depending upon the circumferential wave number and semi-cone angle.
(vi) The degree of snap-through in the post-buckling response is significantly higher when the cylindrical section is joined with smaller edge of the conical sections.
(vii) The linear eigenvalue analysis overestimates the critical temperature parameter compared to that from nonlinear analysis for shell combinations having joint between larger edge side of the conical-section and cylinder whereas for other cases former one under predicts the critical temperature parameter values.
(viii) The percentage difference between eigenvalue and nonlinear prediction of bifurcation temperature increases with the increase in the semi-cone angle of the joined shells.

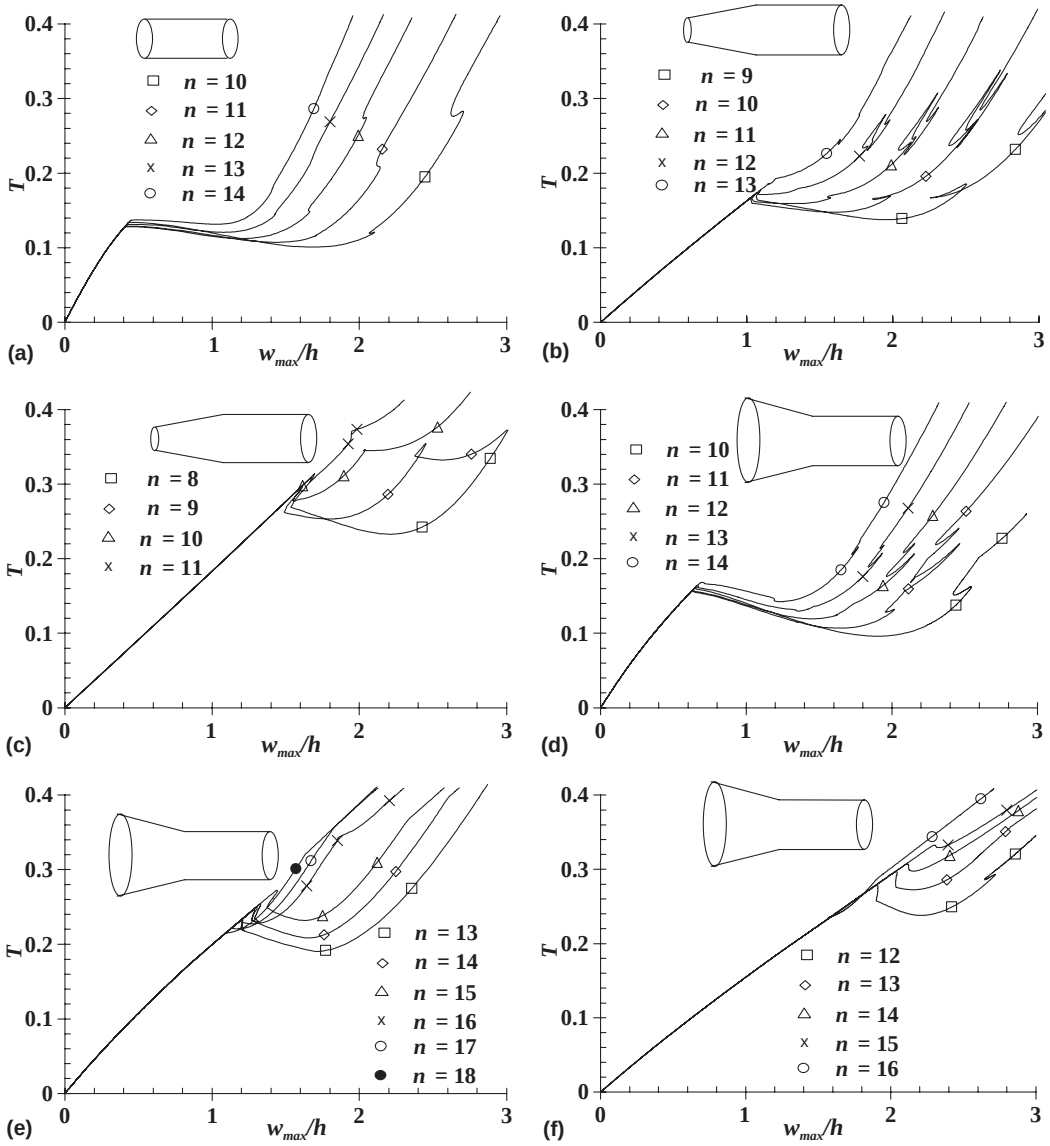

Fig. 11. Maximum displacement ($w_{\max}/h$) versus temperature parameter (T) curves for cross-ply laminated joined conical–cylindrical shells (Material 1): (a) $\phi = 0°$; (b) $\phi = 15°$; (c) $\phi = 30°$; (d) $\phi = -15°$; (e) $\phi = -30°$; (f) $\phi = -45°$.

(ix) The post-buckling deformation shapes for the joined shell configurations may change significantly along the equilibrium path with the starting of the conversion of membrane energy to bending one near the joint and then progressing in the full shell.

(x) The post-buckling stiffness of the shells may decrease with orthotropicity ratio of material specifically along the lowest post-buckling curves among different circumferential wave number (n).

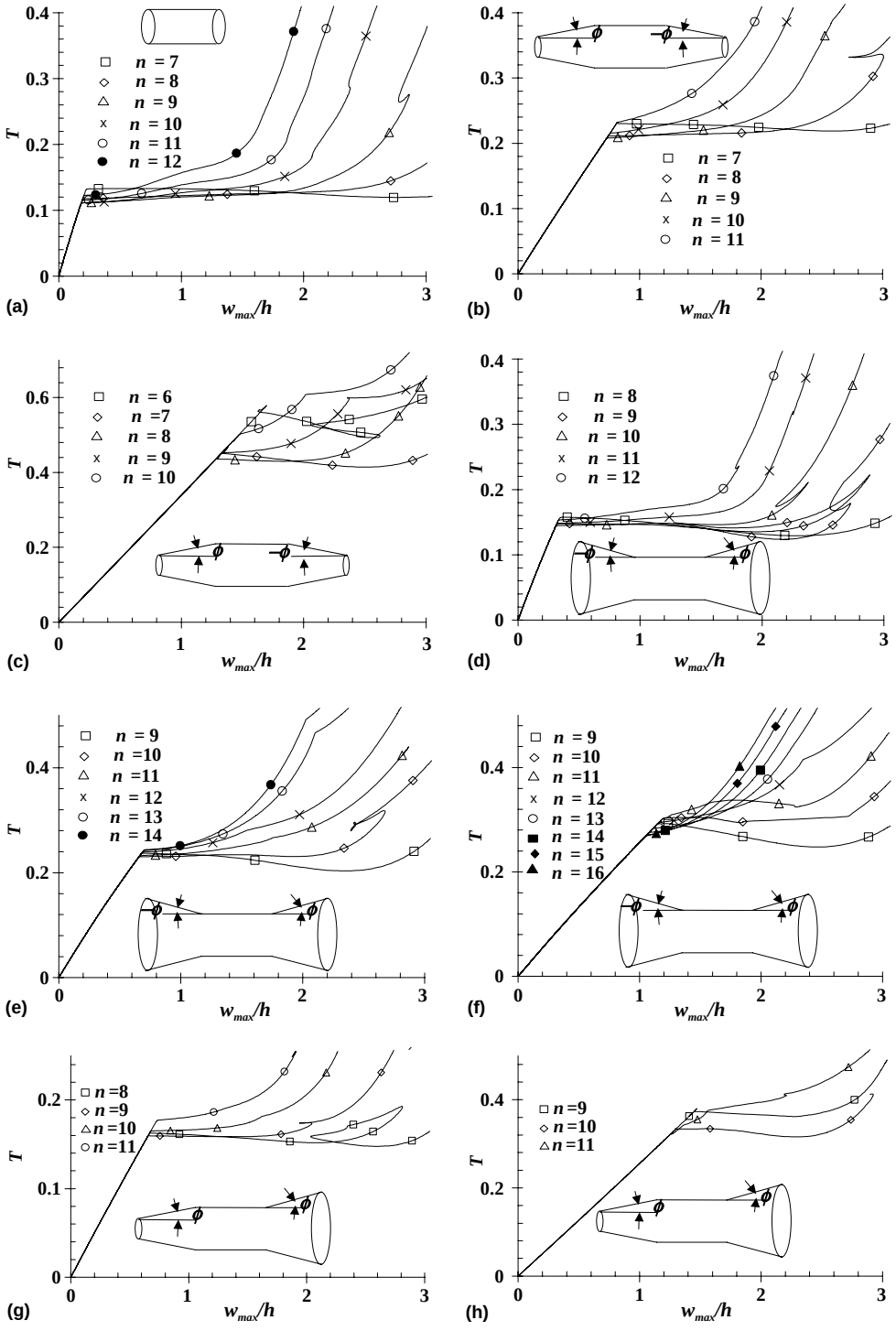

Fig. 12. Maximum displacement (w_{max}/h) versus temperature parameter (T) curves for cross-ply laminated joined conical–cylindrical–conical shells (Material 2): (a) $\phi = 0°$; (b) $\phi = 15°$; (c) $\phi = 30°$; (d) $\phi = -15°$; (e) $\phi = -30°$; (f) $\phi = -45°$; (g) $\phi = 15°$; (h) $\phi = 30°$.

References

Amabili, M., Pellicano, F., Paidoussis, M.P., 1999. Non-linear dynamics and stability of circular cylindrical shells containing flowing fluid, Part II: Large amplitude vibrations without flow. Journal of Sound and Vibration 228, 1103–1124.

Anwen, W., 1998. Stresses and stability for the cone–cylinder shells with toroidal transition. International Journal of Pressure Vessels and Piping 75, 49–56.

Argyris, J.H., Tenek, L., 1997. Recent advances in computational thermostructural analysis of composite plates and shells with strong nonlinearities. Applied Mechanics Reviews 50 (5), 285–305.

Batoz, J.L., Dhatt, G., 1979. Incremental displacement in nonlinear analysis. International Journal for Numerical Methods in Engineering 14, 1262–1267.

Bergan, P.G., Clough, R.W., 1972. Convergence criteria for iterative process. AIAA Journal 10, 1107–1108.

Flores, F.G., Godoy, L.A., 1991. Post-buckling of elastic cone–cylinder and sphere-cylinder complex shells. International Journal of Pressure Vessels and Piping 45, 237–258.

Kraus, H., 1976. Thin Elastic Shells. John Wiley, New York.

Noor, A.K., Burton, W.S., 1992. Computational models for high-temperature multilayered composite plates and shells. Applied Mechanics Reviews 45 (10), 419–446.

Patel, B.P., Ganapathi, M., Makhecha, D.P., Shah, P., 2003. Large amplitude free flexural vibration of rings using finite element approach. International Journal of Non-Linear Mechanics 37, 911–921.

Patel, B.P., Shukla, K.K., Nath, Y., 2004. Thermal buckling of laminated cross-ply oval cylindrical shells. Composite Structures 65, 217–229.

Patel, B.P., Shukla, K.K., Nath, Y., in press. Thermal postbuckling analysis of laminated cross-ply truncated circular conical shells. Composite Structures. Available form: <www.sciencedirect.com>.

Patel, B.P., Shukla, K.K., Nath, Y., 2005. Thermal postbuckling of laminated conical shells with temperature dependent material properties. AIAA Journal 43 (6), 1380–1388.

Teng, J.G., 1994. Cone–cylinder intersection under internal pressure: axisymmetric failure. Journal of Engineering Mechanics, ASCE 120, 1896–1912.

Teng, J.G., 1995. Cone–cylinder intersection under internal pressure: nonsymmetric buckling. Journal of Engineering Mechanics, ASCE 121, 1298–1305.

Teng, J.G., 1996. Elastic buckling of cone–cylinder intersection under localized circumferential compression. Engineering Structures 18, 41–48.

Teng, J.G., Ma, H.-W., 1999. Elastic buckling of ring-stiffened cone–cylinder intersections under internal pressure. International Journal of Mechanical Sciences 41, 1357–1383.

Thornton, E.A., 1993. Thermal buckling of plates and shells. Applied Mechanics Reviews 46 (10), 485–506.

Tong, P., Pian, T.H.H., 1974. Postbuckling analysis of shells of revolution by the finite element method. In: Fung, Y.C., Sechler, E.E. (Eds.), Thin Shell Structures. Prentice-Hall, Upper Saddle River, NJ, pp. 435–452.

Ueda, T., 1979. Nonlinear free vibrations of conical shells. Journal of Sound and Vibration 64, 85–95.

Zhao, Y., Teng, J.G., 2003. A stability design proposal for cone–cylinder intersections under internal pressure. International Journal of Pressure Vessels and Piping 80, 297–309.